

## ARTICLE



# PTPRZ1 dephosphorylates and stabilizes RNF26 to reduce the efficacy of TKIs and PD-1 blockade in ccRCC

Yongkang Ma<sup>1,11</sup>, Wei Li<sup>2,3,4,11</sup>, Xinlin Liu<sup>5</sup>, Weilin Peng<sup>5</sup>, Bei Qing<sup>5</sup>, Shangqing Ren<sup>6</sup>, Wentao Liu<sup>7,8,9,10</sup> and Xiaobing Chen<sup>7,8,9,10</sup>

© The Author(s), under exclusive licence to Springer Nature Limited 2024

Clear cell renal cell carcinoma (ccRCC), the most common subtype of renal cell carcinoma, often exhibits resistance to tyrosine kinase inhibitors (TKIs) when used as monotherapy. However, the integration of PD-1 blockade with TKIs has significantly improved patient survival, making it a leading therapeutic strategy for ccRCC. Despite these advancements, the efficacy of this combined therapy remains suboptimal, necessitating a deeper understanding of the underlying regulatory mechanisms. Through comprehensive analyses, including mass spectrometry, RNA sequencing, lipidomic profiling, immunohistochemical staining, and ex vivo experiments, we explored the interaction between PTPRZ1 and RNF26 and its impact on ccRCC cell behavior. Our results revealed a unique interaction where PTPRZ1 stabilized RNF26 protein expression by dephosphorylating it at the Y432 site. The modulation of RNF26 levels by PTPRZ1 was found to be mediated through the proteasome pathway. Additionally, PTPRZ1, via its interaction with RNF26, activated the TNF/NF- $\kappa$ B signaling pathway, thereby promoting cell proliferation, angiogenesis, and lipid metabolism in ccRCC cells. Importantly, inhibiting PTPRZ1 enhanced the sensitivity of ccRCC to TKIs and PD-1 blockade, an effect that was attenuated when RNF26 was simultaneously knocked down. These findings highlight the critical role of the PTPRZ1-RNF26 axis in ccRCC and suggest that combining PTPRZ1 inhibitors with current TKIs and PD-1 blockade therapies could significantly improve treatment outcomes for ccRCC patients.

*Oncogene*; <https://doi.org/10.1038/s41388-024-03198-8>

## INTRODUCTION

Clear cell renal cell carcinoma (ccRCC) is the predominant pathological subtype of renal cell carcinoma (RCC), accounting for about three-quarters of RCC cases [1]. The 5-year survival rate for patients diagnosed with metastatic ccRCC is approximately 12% [2]. Systemic therapy is the standard treatment for ccRCC. The hyperactivation of angiogenesis-related signaling pathways, due to loss-of-function mutations in Von Hippel-Lindau (VHL) genes and the accumulation of hypoxia-inducible factor (HIF), is characteristic of ccRCC. Tyrosine kinase inhibitors (TKIs), including sunitinib, sorafenib, axitinib, lenvatinib, and pazopanib, target the vascular endothelial growth factor (VEGF) axis and inhibit angiogenesis, and are approved for treating ccRCC [3–6]. However, clinical practice reveals that TKI treatment alone is insufficient for ccRCC patients due to primary and acquired resistance [7]. Immune checkpoint therapy, such as programmed death-1 (PD-1) blockade, is introduced to treat ccRCC patients [7]. The combination of PD-1 blockade and TKIs improves the survival rate and becomes the first-line therapeutic strategy for ccRCC. Notably, the response rate to combined TKI/PD-1 blockade treatment still

does not exceed 50% [8]. Thus, it is necessary to explore the underlying mechanisms regulating the efficacy of TKI/PD-1 blockade treatment in ccRCC.

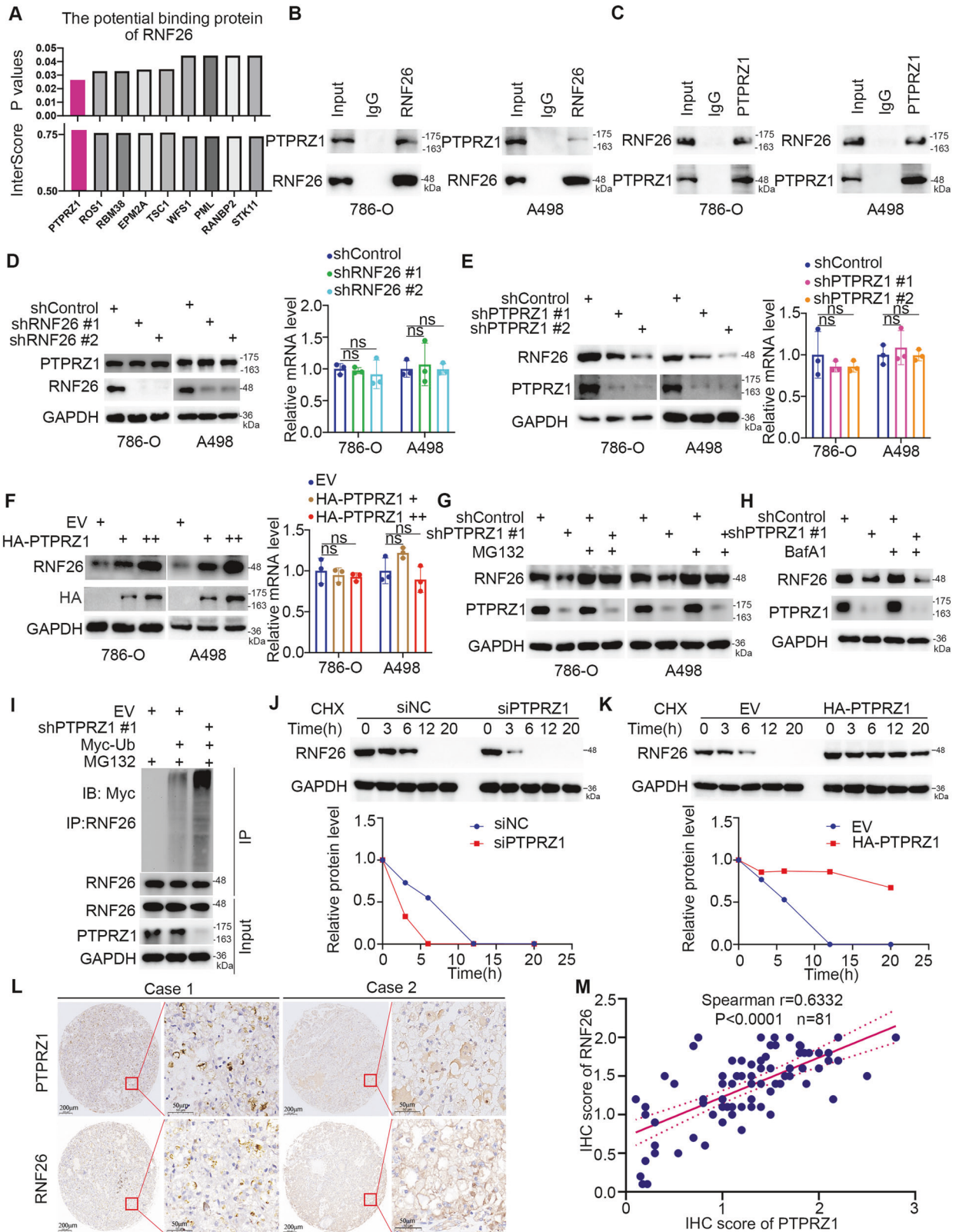
RING finger protein 26 (RNF26) is an endoplasmic reticulum transmembrane E3 ligase responsible for modulating the endolysosomal pathway [9, 10]. It has been reported that aberrantly overexpressed RNF26 promotes the proliferation of pancreatic cancer cells by degrading RBM38 [11]. Similarly, we reported that RNF26 functions as a tumor growth-promoting protein by decreasing the protein levels of p57 in bladder cancer [12]. Our findings also suggest that RNF26 is crucial for modulating the sensitivity of ccRCC to TKIs, mTOR inhibitors, and PD-1 blockade through the dysregulation of the TNF and mTOR signaling pathways [13]. Therefore, RNF26 is an ideal candidate for improving the efficacy of TKI/PD-1 blockade treatment in ccRCC.

Considering that no direct drugs target RNF26, further exploration of the regulatory mechanisms of RNF26 in ccRCC is needed. Here, we screened potential binding proteins of RNF26 and found that protein tyrosine phosphatase receptor zeta 1 (PTPRZ1), a transmembrane tyrosine phosphatase, interacts with

<sup>1</sup>Department of Urology, Affiliated Cancer Hospital of Zhengzhou University, Henan Cancer Hospital, Zhengzhou, China. <sup>2</sup>Department of Urology, The Second Xiangya Hospital, Central South University, Changsha, Hunan 410011, China. <sup>3</sup>Uro-Oncology Institute of Central South University, Changsha, Hunan 410011, China. <sup>4</sup>Hunan Engineering Research Center of Smart and Precise Medicine, Changsha, Hunan 410011, China. <sup>5</sup>Department of Thoracic Surgery, The Second Xiangya Hospital of Central South University, Changsha, Hunan, China. <sup>6</sup>Robotic Minimally Invasive Surgery Center, Sichuan Provincial People's Hospital, School of Medicine, University of Electronic Science and Technology of China, Chengdu 610072, China. <sup>7</sup>Department of Medical Oncology, Affiliated Cancer Hospital of Zhengzhou University, Henan Cancer Hospital, Zhengzhou, Henan Province, China. <sup>8</sup>State Key Laboratory of Esophageal Cancer Prevention & Treatment, Zhengzhou University, Zhengzhou, Henan Province, China. <sup>9</sup>Henan Engineering Research Center of Precision Therapy of Gastrointestinal Cancer, Zhengzhou, Henan Province, China. <sup>10</sup>Zhengzhou Key Laboratory for Precision Therapy of Gastrointestinal Cancer, Zhengzhou, Henan Province, China. <sup>11</sup>These authors contributed equally: Yongkang Ma, Wei Li, Xinlin Liu. ✉email: [rsq0516@163.com](mailto:rsq0516@163.com); [xyeylwt@csu.edu.cn](mailto:xyeylwt@csu.edu.cn); [zlyyichenxb0807@zzu.edu.cn](mailto:zlyyichenxb0807@zzu.edu.cn)

Received: 9 July 2024 Revised: 10 October 2024 Accepted: 14 October 2024

Published online: 23 October 2024



and dephosphorylates RNF26 at the Y432 site to prevent RNF26 degradation. Recent studies indicate that PTPRZ1 overexpression promotes tumor progression in glioblastoma through HOXA5-induced mechanisms [14], and activates NF-kappa B pathways to enhance glioblastoma cell migration [15]. A soluble cleaved form

of PTPRZ1 serves as a diagnostic marker for glioma due to its increased presence in cerebrospinal fluid [16]. Additionally, PTPRZ1 is a substrate of VHL E3 ligase, with VHL loss-of-function mutations leading to PTPRZ1 accumulation in ccRCC [17]. Moreover, HIF-2, but not HIF-1, upregulates PTPRZ1 expression in

**Fig. 1 PTPRZ1 binds to and stabilizes RNF26 in ccRCC.** **A** Proteins were extracted from 786-O cells, magnetic beads and RNF26 antibodies were used for co-immunoprecipitation (Co-IP) and mass spectrometry was performed to detect proteins interacting with RNF26. **B, C** The whole cell lysate (WCL) of 786-O and A498 cells were harvested for Co-Immunoprecipitation (Co-IP) assay. **D, E** 786-O and A498 cells were infected with indicated shRNAs for 72 h, cells were harvested for the western blot analysis and RT-qPCR analysis. Data present as mean  $\pm$  SD with three replicates. ns, not significant. **F** 786-O and A498 cells were transfected with indicated plasmids for 24 h, cells were harvested for the western blot analysis and RT-qPCR analysis. Data present as mean  $\pm$  SD with three replicates. ns, not significant. **G, H** 786-O and A498 cells were infected with indicated shControl or shPTPRZ1 for 72 h, and treated with or without MG132 and BafA1 respectively for 24 h, cells were harvested for the western blot analysis. **I** A498 cells were infected with indicated shRNAs and plasmid for 72 h, and treated with or without MG132 for 24 h, cells were harvested for the western blot analysis. **J, K** A498 and 786-O cells were transfected with indicated siRNAs for 48 h (**J**) or plasmids for 24 h (**K**) and treated with CHX, cells were harvested for the western blot analysis and RT-qPCR analysis at different time points. **L, M** IHC analysis of the renal cancer tissue microarray (renal cancer and paracancer tissue specimens,  $n = 81$ ) by staining the PTPRZ1 or RNF26 antibodies. The typical images are shown in panel L. The scale bar indicated in the panel L was 200  $\mu$ m and 50  $\mu$ m, respectively. The IHC scoring were performed and the correlation between IHC score of PTPRZ1 and RNF26 were analysed (**M**). *P*-value as indicated.

HEK293T cells under hypoxic conditions [18]. PTPRZ1 is reported to be a substrate of VHL and is overexpressed in RCC due to VHL inactivation [17, 19]. Overexpressed PTPRZ1 promotes ccRCC cell proliferation by dephosphorylating beta-catenin [17, 19]. We also showed that PTPRZ1 modulates lipid metabolism and activates the NF-kappa B signaling pathway through RNF26 in ccRCC. Lastly, inhibition of PTPRZ1 was found to increase the anti-tumor effect of TKIs and PD-1 blockade in ccRCC.

## RESULTS

### PTPRZ1 binds to and stabilizes RNF26 in ccRCC

Through analysis of the protein-protein interaction network, we identified PTPRZ1 as a potential binding partner of RNF26 (Fig. 1A), with RBM38 and TSC1 serving as positive controls [11] (Fig. 1A). Subsequent co-immunoprecipitation (co-IP) experiments confirmed that endogenously expressed RNF26 interacts with PTPRZ1 in ccRCC cells (Fig. 1B, C). Further investigation revealed that knockdown of RNF26 did not affect PTPRZ1 expression in ccRCC cells (Fig. 1D), suggesting that PTPRZ1 is not degraded by RNF26. Conversely, depletion of PTPRZ1 reduced the protein levels, but not the mRNA levels, of RNF26 in ccRCC cells (Fig. 1E), whereas overexpression of PTPRZ1 increased RNF26 protein levels (Fig. 1F). Additionally, proteasome inhibitors (MG132), but not lysosome inhibitors (BafA1), prevented the reduction of RNF26 protein following PTPRZ1 knockdown (Fig. 1G, H). Further analysis demonstrated that PTPRZ1 depletion promoted poly-ubiquitination and reduced the half-life of RNF26 protein in ccRCC cells (Fig. 1I, J), while overexpression of PTPRZ1 extended the protein half-life of RNF26 in 786-O cells, with the value at 0 h serving as a reference point for comparison (Fig. 1K). Using immunohistochemical (IHC) staining with PTPRZ1 and RNF26 antibodies on RCC tissue microarrays comprising 81 tumor and adjacent non-tumor tissues revealed a positive correlation between RNF26 and PTPRZ1 protein levels (Fig. 1L, M). Collectively, these findings suggest that PTPRZ1 regulates the protein stability of RNF26 in ccRCC.

### PTPRZ1 dephosphorylates RNF26 at Y432 site

Given that PTPRZ1 functions as a tyrosine phosphatase, we investigated whether PTPRZ1 dephosphorylates RNF26 to modulate its stability in ccRCC. Overexpression of PTPRZ1 decreased the total tyrosine phosphorylation levels of RNF26 in 786-O cells (Fig. 2A), while knockdown of PTPRZ1 increased these levels (Fig. 2B). The PhosphoSitePlus web tool predicted that the Y432 site of RNF26 might be phosphorylated (Fig. 2C). It has been reported that the amount of RNF26 is auto-regulated by ubiquitin-proteasome dependent degradation [20]. The mutagenesis of RNF26 at the Y432 site led to 4-fold increase of stability [20]. We constructed a Flag-RNF26 Y432A mutant plasmid to mimic the dephosphorylated state of RNF26 at Y432. Overexpressing PTPRZ1 with the RNF26 Y432A mutant did not further decrease the total tyrosine phosphorylation levels compared to wild-type (WT) RNF26 in 786-O cells (Fig. 2D). Knockdown or inhibition of PTPRZ1

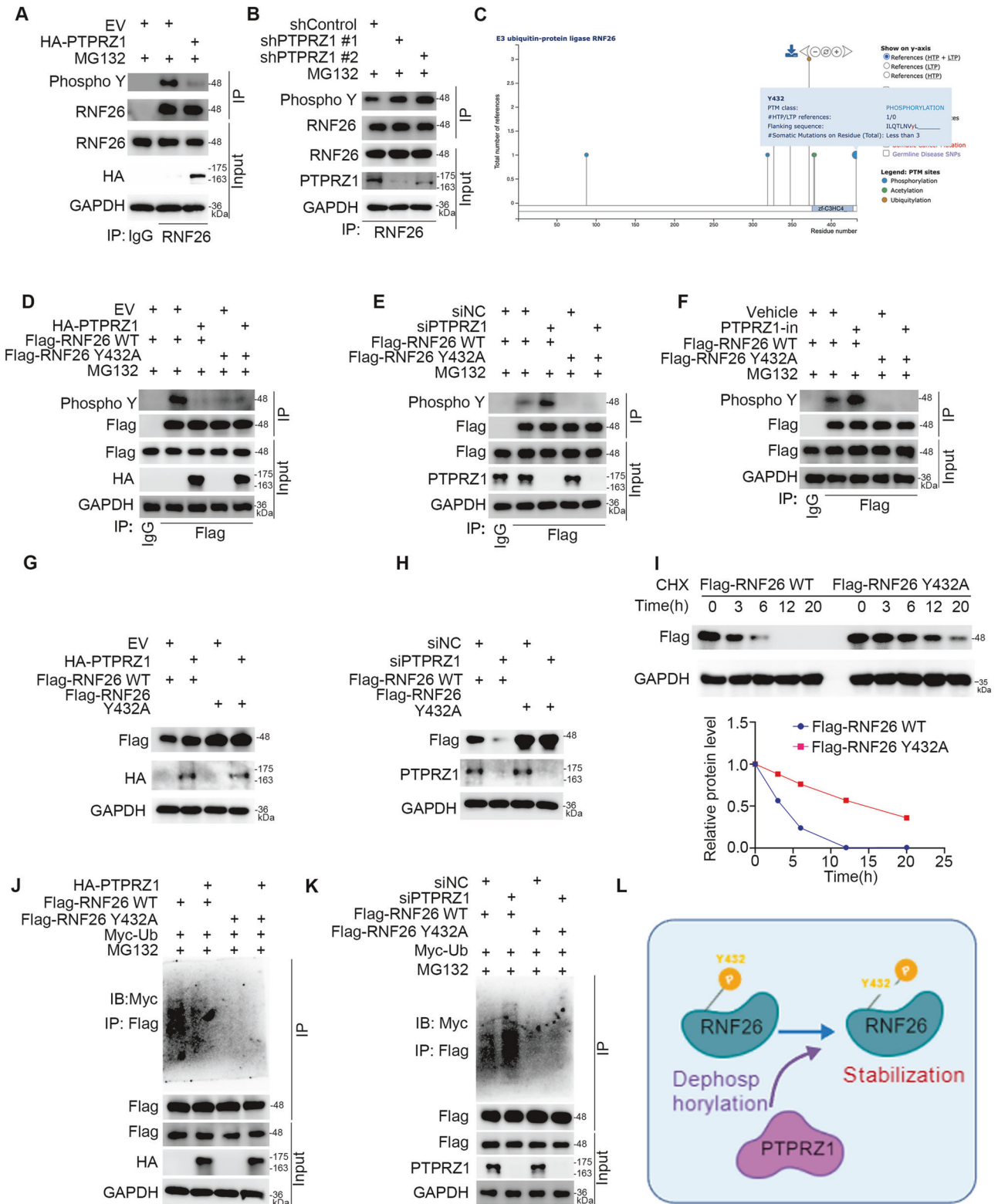
did not increase tyrosine phosphorylation levels in RNF26 Y432A mutants (Fig. 2E, F). Additionally, the RNF26 Y432A mutant increased RNF26 protein levels and reduced the effect of PTPRZ1 on RNF26 stability in ccRCC cells compared to WT RNF26 (Fig. 2G, H). In consistent with previous findings [20], the RNF26 Y432A mutant exhibited a longer protein half-life and lower poly-ubiquitination levels than WT RNF26 in 786-O cells (Fig. 2I–K). Overexpression of PTPRZ1 did not further decrease poly-ubiquitination levels of RNF26 in 786-O cells (Fig. 2J). Relatively, knocking down PTPRZ1 also yielded corresponding experimental results (Fig. 2K). Thus, PTPRZ1 promotes RNF26 stabilization by dephosphorylating it at Y432 in ccRCC cells (Fig. 2L).

### PTPRZ1 contributes to the activation of the TNF and NF-kappa B signaling pathways in ccRCC cells

Given that PTPRZ1 was reported to be aberrantly up-regulated in RCC and enhance the cell proliferation of ccRCC [17, 19]. We were plan to further study the role and related mechanism of PTPRZ1 in ccRCC. Similarly, We confirmed that PTPRZ1 protein levels in RCC tissues were higher than in adjacent non-tumor tissues (Fig. 3A, B). Then, PTPRZ1 was found to promote the ccRCC cells growth and angiogenesis (Fig. 3C–E and Supplementary Fig. 1A–J). Analysis of the TCGA-KIRC dataset showed a positive correlation between PTPRZ1 and the renal cell carcinoma and NF-kappa B signaling pathways (Fig. 3F, G). The RNA-seq was performed after knockdown of PTPRZ1 in 786-O cells (Fig. 3H). GSEA and KEGG enrichment analysis indicated that PTPRZ1 was involved in activation of pathways including DNA replication, cell cycle, EGFR-tyrosine kinase inhibitor resistance, renal cell carcinoma, TNF signaling, and NF-kappa B signaling (Fig. 3I–K). We previously reported that RNF26 activates TNF signaling pathway to decrease the sensitivity of ccRCC cells to sunitinib [13]. Since the above data showed that PTPRZ1 prevented RNF26 from degradation, we examined its role in regulating the TNF/NF-kappa B signaling pathways in ccRCC. Notably, we showed that knockdown or inhibitors of PTPRZ1 decreased p65 phosphorylation, while overexpression of PTPRZ1 increased it in ccRCC cells (Fig. 3L, M and Supplementary 1K). In addition, we showed that depletion of PTPRZ1 reduced the expression of TNF/NF-kappa B pathway genes such as *CXCL1* or *PTGS2*, and this effect was attenuated by p65 inhibitors (e.g., JSH-23) in ccRCC cells (Fig. 3N and Supplementary 1L). Overexpression of PTPRZ1 elevated TNF/NF-kappa B pathway gene expression, and this effect was also diminished by JSH-23 in ccRCC cells (Fig. 3O and Supplementary 1M). Together, our data suggest that PTPRZ1 is responsible for the activation of TNF/ NF-kappa B signaling pathway in ccRCC.

### PTPRZ1 regulates the lipid metabolism of ccRCC cells

According to the RNA-seq in 786-O cells (Fig. 3H), we observed that lipid metabolism-related pathways, such as fat digestion and absorption, ether lipid metabolism, and cholesterol metabolism, were inactivated following PTPRZ1 knockdown (Fig. 3I–K). Dysregulation of lipid metabolism is a hallmark of ccRCC, contributing to



reduced sensitivity to TKIs and PD-1 blockade [21, 22]. It has been reported that the NF-kappa B signaling pathway modulated the lipid metabolism in cells [23]. We investigated whether PTPRZ1 regulates lipid metabolism via the NF-kappa B pathway. Non-targeted lipidomics analysis after PTPRZ1 knockdown in 786-O cells revealed changes in lipid metabolism components (Fig. 4A). The KEGG enrichment analysis of changed components associated with

the lipid metabolism suggested that these components were closely associated with Glycosylphosphatidylinositol (GPI)-anchor biosynthesis (1-Phosphatidyl-D-myo-inositol and Phosphatidylethanolamine), Ether lipid metabolism (1-Alkyl-2-acylglycerophosphoethanolamine and 1-Radyl-2-acyl-sn-glycero-3-phosphocholine), Fat digestion and absorption (Phosphatidate), and Pathways in cancer (Phosphatidate), which was consistent with

**Fig. 2 PTPRZ1 dephosphorylates RNF26 at Y432 site.** **A** A498 cells were transfected with EV or HA-PTPRZ1 plasmids for 24 h, cells were harvested for IP and the western blot analysis. **B** A498 cells were infected with shControl or shPTPRZ1 for 72 h, cells were harvested for IP and the western blot analysis. **C** The PhosphoSitePlus web tool predicted the phosphorylation modification site of RNF26. **D** A498 cells were transfected with indicated plasmids and treated with MG132 for 24 h, cells were harvested for IP and the western blot analysis. **E** A498 cells were transfected with indicated plasmids for 24 h and siRNAs for 48 h, and treated with MG132 for 24 h, cells were harvested for IP and the western blot analysis. **F** A498 cells were transfected with indicated plasmids for 24 h, and treated with inhibitor of PTPRZ1 (NAZ2329) and MG132 for 24 h, cells were harvested for IP and the western blot analysis. **G, H** A498 cells were transfected with indicated plasmids for 24 h (**G**) and siRNAs for 48 h (**H**), cells were harvested for the western blot analysis. **I** A498 cells were transfected with indicated plasmids for 24 h, and treated with CHX, cells were harvested for the western blot analysis and RT-qPCR analysis at different time points. **J, K** A498 cells were transfected with indicated plasmid for 24 h (**J**) or siRNA for 48 h (**K**), and treated with MG132 for 24 h, cells were harvested for the IP and the western blot analysis. **L** A model depicting that PTPRZ1 mediated the Y432 phosphorylation of RNF26 to stabilize the expression of RNF26.

the RNA-seq data in Fig. 3 (Fig. 4B). Then, the oil-red staining was applied to preliminary study the role of PTPRZ1 on the regulation of lipid metabolism. We showed that knockdown of PTPRZ1 reduced the amount of lipid droplets in ccRCC cells, while overexpression of PTPRZ1 increased the amount of lipid droplets in ccRCC cells (Fig. 4C–E). The effect of PTPRZ1 on lipid droplets amount was diminished by NF-kappa B inhibitors (JSH-23 or IKK-16) (Fig. 4F, G). Together, these findings suggest that PTPRZ1 regulates lipid metabolism in ccRCC cells.

### RNF26 is the key mediator for PTPRZ1 in ccRCC

Given that RNF26 has been documented to activate TNF/NF-kappa B signaling pathways in ccRCC, we aimed to explore whether RNF26 serves as a crucial mediator of PTPRZ1 in this context. Similarly, the RNA-seq analysis after knockdown of RNF26 (GSE23944066) indicated that RNF26 also associated with the lipid metabolism related pathways, such as ether lipid metabolism and fat digestion and absorption (Fig. 5A). The combined analysis of the RNA-seq after knockdown of PTPRZ1 or RNF26 to show that there were 463 + 328 genes co-related by PTPRZ1 and RNF26 in ccRCC cells (Fig. 5B). Gene Set Enrichment Analysis (GSEA) demonstrated that these genes were linked to metabolic pathways, NF-kappa B signaling, cell cycle regulation, TNF signaling, and cancer-related pathways (Fig. 5C). Additionally, KEGG enrichment analysis highlighted these genes involvement in NF-kappa B signaling, TNF signaling, EGFR tyrosine kinase inhibitor resistance, and PD-L1 expression in the PD-1 checkpoint pathway (Fig. 5D). Then, we showed that changing the expression of PTPRZ1 led to the changing of the target proteins of RNF26, such as p57 and CBX7, and phosphorylation of p65, which was diminished by co-knockdown of RNF26 in ccRCC cells (Fig. 5E, F). Moreover, co-knockdown of RNF26 attenuated PTPRZ1's regulation of TNF/NF-kappa B signaling pathway genes, including *CXCL1* and *PTGS2*, and its effects on cell proliferation, lipid accumulation and angiogenesis (Fig. 5G–M, Supplementary 1N). Collectively, these findings collectively suggest that PTPRZ1 activates TNF/NF-kappa B signaling pathways, promoting cell proliferation and angiogenesis partly through RNF26 in ccRCC.

### PTPRZ1 decreases the anti-tumor effect of ccRCC to TKIs and PD-1 blockade

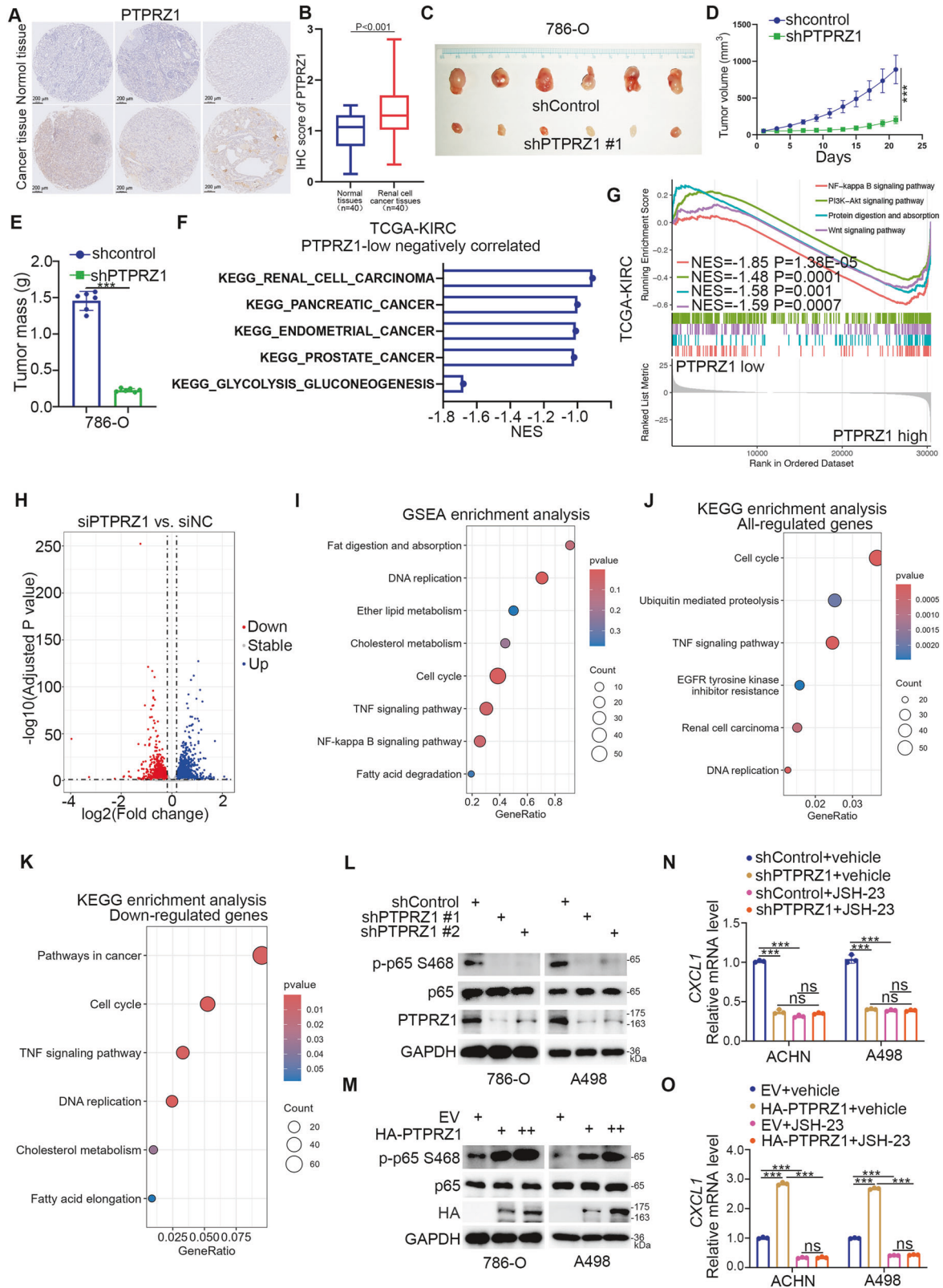
Aberrantly expressed RNF26 and hyper-activated TNF/NF-kappa B signaling pathways are closely associated with reduced sensitivity of ccRCC to TKIs and PD-1 blockade [13, 24]. Building upon these findings, which illustrate PTPRZ1's role in regulating RNF26 stability and activating TNF/NF-kappa B signaling, we investigated whether PTPRZ1 influences ccRCC sensitivity to TKIs and PD-1 blockade. First, our data showed that depletion of PTPRZ1 increased PD-1 blockade sensitivity and CD8 + T-cell infiltration in the tumor microenvironment in an immunocompeted mouse model, and this effect can be diminished by knockdown of RNF26 (Fig. 6A–F). Meanwhile, Our results show that knockdown or inhibitors of PTPRZ1 decreased the IC50 of sunitinib and lenatinib in ccRCC cells (Fig. 6G, Supplementary 2A–D). In contrast, ectopically overexpression of PTPRZ1 increased the IC50 of

sunitinib and lenatinib in ccRCC cells (Fig. 6H and Supplementary 2E). Further studies demonstrated that RNF26 co-knockdown attenuated IC50 changes induced by PTPRZ1 overexpression in A498 and 786-O cells, where co-knockdown did not significantly decrease additional IC50 values of sunitinib and lenvatinib compared to PTPRZ1 knockdown alone (Fig. 6I, J, Supplementary 2F, G). However, the results of the nude mice experiments demonstrated that co-knockdown of PTPRZ1 and RNF26 inhibited tumor growth in vivo more effectively with the concomitant addition of lenvatinib compared to the knockdown of PTPRZ1 alone (Fig. 6K–M). Together, these data suggest that PTPRZ1 regulates the sensitivity of ccRCC to TKIs (sunitinib and lenvatinib) and ICIs (PD-1 blockade). PTPRZ1 stabilizes RNF26 by dephosphorylating its Y432 site, activates TNF/NF-kappa B signaling pathways to modulate lipid metabolism and enhance proliferation and angiogenesis in ccRCC cells, thereby reducing sensitivity to TKIs and PD-1 blockade, highlighting PTPRZ1 inhibition as a potential therapeutic strategy for ccRCC (Supplementary 3A).

### DISCUSSION

Patients with advanced ccRCC receiving combined TKI and PD-1 blockade therapy exhibit better prognosis than those receiving TKIs alone. Previous studies have indicated that RNF26 regulates ccRCC sensitivity to sunitinib via the CBX7-TNF signaling pathway and modulates PD-L1 expression to affect ccRCC response to PD-1 blockade. Additionally, literature reports indicate RNF26's role in modulating innate immune responses through the cGAS-STING pathways [20], making it a potential candidate to enhance ccRCC sensitivity to TKIs and PD-1 blockade. However, direct inhibitors targeting RNF26 function are currently unavailable. Our previous investigations into RNF26's regulatory mechanisms at the transcriptional level revealed that FOXM1, in association with LIN9, LIN54, and MuvB, enhances RNF26 mRNA levels, which can be inhibited by FOXM1 inhibitors like FDI-6 [12]. Moreover, RNF26 is known to undergo instability via ubiquitin-proteasome-dependent degradation, primarily regulated by mutagenesis at the Y432 site. Here, we demonstrate that PTPRZ1 dephosphorylates RNF26 at Y432, thereby preventing its degradation. Inhibitors targeting PTPRZ1 decrease RNF26 protein levels, providing insights into RNF26's regulatory mechanisms in cancer cells and suggesting potential applications of PTPRZ1 inhibitors to enhance ccRCC sensitivity to TKIs and PD-1 blockade. Notably, RNF26 is just one downstream target of FOXM1 and PTPRZ1 inhibitors, suggesting the need for further research into upstream regulatory mechanisms of RNF26.

PTPRZ1 is a membrane protein overexpressed in the central nervous system [16]. The role of PTPRZ1 in cancer is cancer type dependent and controversial. PTPRZ1 overexpression is also observed in primary and metastatic melanomas [25], triple-negative breast cancer [26], cervical carcinoma [27], and epithelial ovarian cancer cells [28]. Conversely, PTPRZ1 expression is downregulated in various cancers, acting as a tumor suppressor gene. Hypermethylation of the PTPRZ1 promoter and reduced mRNA levels are observed in colorectal cancer [29, 30]. while



decreased PTPRZ1 expression is noted in prostate cancer tissues [31]. Consistent with previous reports, our results demonstrate downregulation of PTPRZ1 in ccRCC tissues compared to adjacent non-tumor tissues. Given PTPRZ1's function as a tyrosine phosphatase, its impact on tumors depends on downstream

target proteins. PTPRZ1 is reported to dephosphorylate beta-Catenin, activating Wnt signaling to promote carcinogenesis in ccRCC and oral submucous fibrosis malignancy [19, 32]. Conversely, genetic deletion of PTPRZ1 enhances angiogenesis and tumor growth in lung adenocarcinoma via c-Met activation [33].

**Fig. 3** PTPRZ1 contributes to the activation of the TNF and NF-kappa B signaling pathways in ccRCC cells. **A, B** IHC staining analysis of the tissue microarray of renal cancer by using the PTPRZ1 antibody. The typical image and expression level of PTPRZ1 in the nontumor tissue and bladder cancer tissue were shown. *P*-values as indicated. The scale bar indicated in the **(A)** is 200  $\mu$ m. **C–E** A498 cells were infected with shControl or shPTRRZ1#1 for 72 h, the Puromycin was used to select shRNA-infected positive cells for 48 h. Then, cells were subcutaneously injected into the flank of nude mice. The xenografts were measured for 21 days. The tumour image is showed in **(C)**, the tumour growth curve is indicated in **(D)**, and the tumour mass is showed in **(E)**. Data presented as mean  $\pm$  SD with six replicates. \*\*\**P* < 0.001. **F, G** Analysis of PTPRZ1 in TCGA-KIRC dataset. **H–K** The volcano plot of RNA-seq after knockdown of PTPRZ1 in A498 cells **(H)**. GSEA enrichment analysis **(I)** and KEGG enrichment analysis of differential genes **(J, K)** of RNA-seq data. **L** 786-O and A498 cells were infected with indicated shRNAs for 72 h. Cells were harvested for the western blot analysis. **M** 786-O and A498 cells were transfected with indicated plasmids for 24 h. Cells were harvested for the western blot analysis. **N** 786-O and A498 cells were infected with indicated shRNAs for 72 h, and treated with or without JSH-23 for 24 h, cells were harvested for the RT-qPCR analysis. Data present as mean  $\pm$  SD with three replicates. ns not significant; \*\*\**P* < 0.0001. **O** 786-O and A498 cells were transfected with indicated plasmids for 48 h, and treated with or without JSH-23 for 24 h, cells were harvested for the RT-qPCR analysis. Data present as mean  $\pm$  SD with three replicates. ns not significant; \*\*\**P* < 0.0001.

Here, we identify RNF26 as a novel downstream target protein of PTPRZ1, demonstrating that PTPRZ1 stabilizes RNF26 to activate NF-kappa B signaling. Given the complexity of PTPRZ1's cellular functions, these findings raise questions regarding its role in tumors that warrant further investigation, including potential clinical applications of PTPRZ1 inhibitors in cancer treatment.

Collectively, Our findings identify PTPRZ1 as a binding partner of RNF26, crucial for dephosphorylating and stabilizing RNF26 in ccRCC cells. Subsequently, we demonstrated that PTPRZ1 activates the TNF/NF-kappa B signaling pathway, thereby regulating lipid metabolism and promoting cell proliferation and angiogenesis, partly through its interaction with RNF26 in ccRCC cells. Lastly, we observed that PTPRZ1 regulates the sensitivity of ccRCC to TKIs and PD-1 blockade. These discoveries unveil a novel PTPRZ1-RNF26 axis in ccRCC, laying the groundwork for potential new combination therapies for the disease.

## METHODS

### Cell lines and cell culture

786-O (#SC0154) was purchased from Yuchicell Biology (Shanghai, China). A498 (#CL-0254) and HUVEC (#CL-0122), were obtained from Procell Life Science&Technology (Wuhan, China). All cells were identified by short tandem repeat (STR) profiling and tested for mycoplasma contamination. A498 cells were cultured in MEM medium (#L510KJ, Basalmedia, China) supplemented with 10% fetal bovine serum (FBS) (#FBS-CP500, Newzerum) and 1% penicillin/streptomycin (P/S) (#CTCC-002-072, MeisenCTCC, China). The basic medium for 786-O cells was 1640 culture medium (#CTCC-002-003, MeisenCTCC, China) and for HUVEC was Ham's F-12K culture medium (#PM150910, Procell Life Science & Technology, China). All of these cells were placed in an incubator at 37 °C in 5% CO<sub>2</sub>.

### Chemicals and reagents

MG132 (#S2619), Bafilomycin A1 (BafA1) (#S1413), and JSH-23 (#S7351) were acquired from Selleckchem (Shanghai, China). IKK-16 (#HY-13687) and the PTPRZ1 inhibitor NAZ2329 (#HY-103693) were obtained from MedChemExpress (Shanghai, China). The Flag-RNF26 and HA-PTPRZ1 constructs were generated by inserting the cDNA of ZDHHC2 and AGK into the OmicLink™ Expression Clone vector (CMV Promoter; GeneCopoeia, EX-V0006-M14, USA).

### Western blotting, co-immunoprecipitation (IP) and mass spectrometry (MS)

For the western blot analysis, the harvested cell pellets were treated with 100  $\mu$ L of RIPA protein lysis buffer containing 10  $\mu$ L of protease inhibitor on ice for a minimum of 30 min. The protein concentration was determined using the BCA protein assay kit (P0011, Beyotime, Shanghai, China), and the absorbance of the protein standard curve was measured at 570 nm using a microplate reader to quantify the protein concentration in the samples. Equal amounts of protein were resolved by 10% SDS-PAGE and subsequently transferred onto a PVDF membrane. The membrane was blocked with 5% non-fat dry milk in 0.2% Tween-20 in Tris-buffered saline (TBST) for 1 h at room temperature, followed by overnight incubation with the primary antibody at 4 °C. After washing, the membrane was incubated with a secondary antibody conjugated to horseradish peroxidase, and the

immunoreactive bands were visualized. For the co-immunoprecipitation procedure, the cell precipitates were incubated with 1000  $\mu$ L of RIPA protein lysate supplemented with 100  $\mu$ L of protease inhibitor on ice for a minimum of 30 min. The resulting supernatant was then combined with Protein A and G Agarose beads (P2055, Beyotime, Shanghai, China) along with primary antibodies or IgG, and incubated at 4 °C for 24 h. Following this incubation, the beads underwent six washes with 1 $\times$ TBST, followed by the addition of 60  $\mu$ L of sample loading buffer and subsequent boiling for 5 min. Finally, the samples were analyzed by western blotting and the MS was carried out by Shanghai Bioprofile Biotechnology (China). The antibodies used as follows: PTPRZ1 (#P32947, ProMab Biotechnologies, Inc. 1:1000 dilution), RNF26 (#P31953, ProMab Biotechnologies, Inc. 1:1000 dilution), CBX7 (#P05596, ProMab Biotechnologies, Inc. 1:2000 dilution), NF- $\kappa$ B p65 (#20406, ProMab Biotechnologies, Inc. 1:2000 dilution), Phospho-NF- $\kappa$ B p65 (Ser468) (#82335-1-RR, Proteintech, 1:5000 dilution), p57 (#23317-1-AP, Proteintech, 1:4000 dilution), GAPDH (#60004-1-Ig, Proteintech, 1:50000 dilution).

### Colony formation assays

The cells were enzymatically dissociated into single cells using trypsin and then resuspended in complete culture medium. Subsequently, the single-cell suspension was seeded into a 6-well plate at a density of 100, 200, and 500 cells per well, and maintained under standard conditions at 37 °C with 5% CO<sub>2</sub>. The culture medium was refreshed weekly and completely replaced every two weeks. After washing the cells twice with PBS, they were fixed with paraformaldehyde for 20 min, followed by staining with crystal violet for 30 min. The excess dye solution was washed off, and the number of cell clones was counted. The clone formation rate was calculated as (number of clones/number of inoculated cells)  $\times$  100%.

### Immunofluorescence staining

A498 cells were plated onto glass slides. After fixation with a 4% solution of paraformaldehyde for a duration of 15 min, they were exposed to either CD3 (#17617-1-AP, Proteintech, diluted to 1:200), CD4 (#67786-1-Ig, Proteintech, diluted to 1:300) or CD8 (#66868-1-Ig, Proteintech, diluted to 1:300) antibodies at a temperature of 4 °C for an extended period during the night. Following this, the cells underwent multiple rinses using PBS. Subsequently, they were treated with an appropriate secondary antibody conjugated to a fluorophore for a period of 1 h at ambient temperature in a dark environment. The slides were then thoroughly washed again with PBS and treated with DAPI (#C1002, Beyotime, Shanghai, China) for a brief period of 5 min. The resulting images were acquired through the use of a fluorescence microscope.

### Oil red O (ORO) staining

The cells cultured on cell circle microscope cover glass were initially rinsed with PBS and subsequently treated with 4% paraformaldehyde for 30 min. Subsequently, the samples were immersed in 60% isopropyl alcohol for 3 min, followed by staining with freshly prepared 60% Oil Red O solution (prepared by dissolving 0.5 g of Oil Red O in 100 ml of isopropyl alcohol) for 30 min. After that, the samples were briefly rinsed in 60% isopropyl alcohol for 1 min and washed with PBS. Hematoxylin was used for counterstaining. The slides were examined using an Olympus microscope (CX-31, Olympus, Japan). The quantification of the number and size of lipid droplets (LDs) was performed using Image J software according to established protocols (For Oil Red O staining, a minimum of one hundred cells from each group were analyzed).

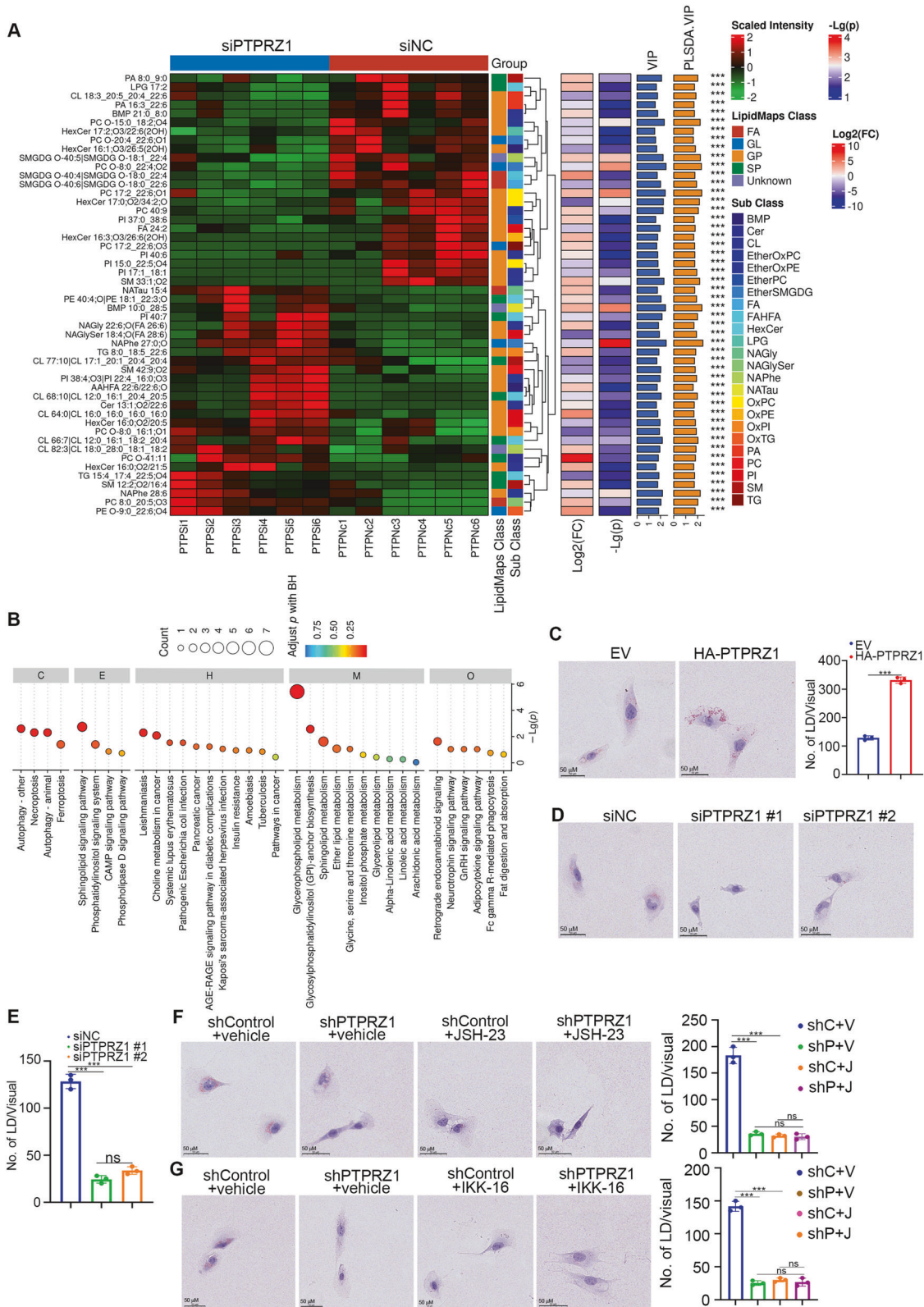


**Fig. 4 PTPRZ1 regulates the lipid metabolism of ccRCC cells.** **A** The heat map of non-targeted lipidomics analysis after knockdown of PTPRZ1 in 786-O cells. **B** KEGG enrichment analysis of clustered components associated with the lipid metabolism of PTPRZ1. **C–E** A498 cells were transfected with indicated plasmids (**C**) or siRNAs (**D, E**) for 48 h, and oil red staining was performed to observe the number of lipid droplet under per view. Data were expressed as mean  $\pm$  SD with three replicates. ns, not significant; \*\*\*,  $P < 0.0001$ . The scale bar indicated in the (**C, D**) was 50  $\mu$ m. **F, G** A498 cells were infected with indicated shRNAs for 72 h, and treated with JSH-23 (**F**) or IKK-16 (**G**) respectively for 24 h, and oil red staining was performed to observe the number of lipid droplet under per view. Data were expressed as mean  $\pm$  SD with three replicates. ns - not significant; \*\*\* $P < 0.0001$ . The scale bar indicated in the (**F, G**) was 50  $\mu$ m.

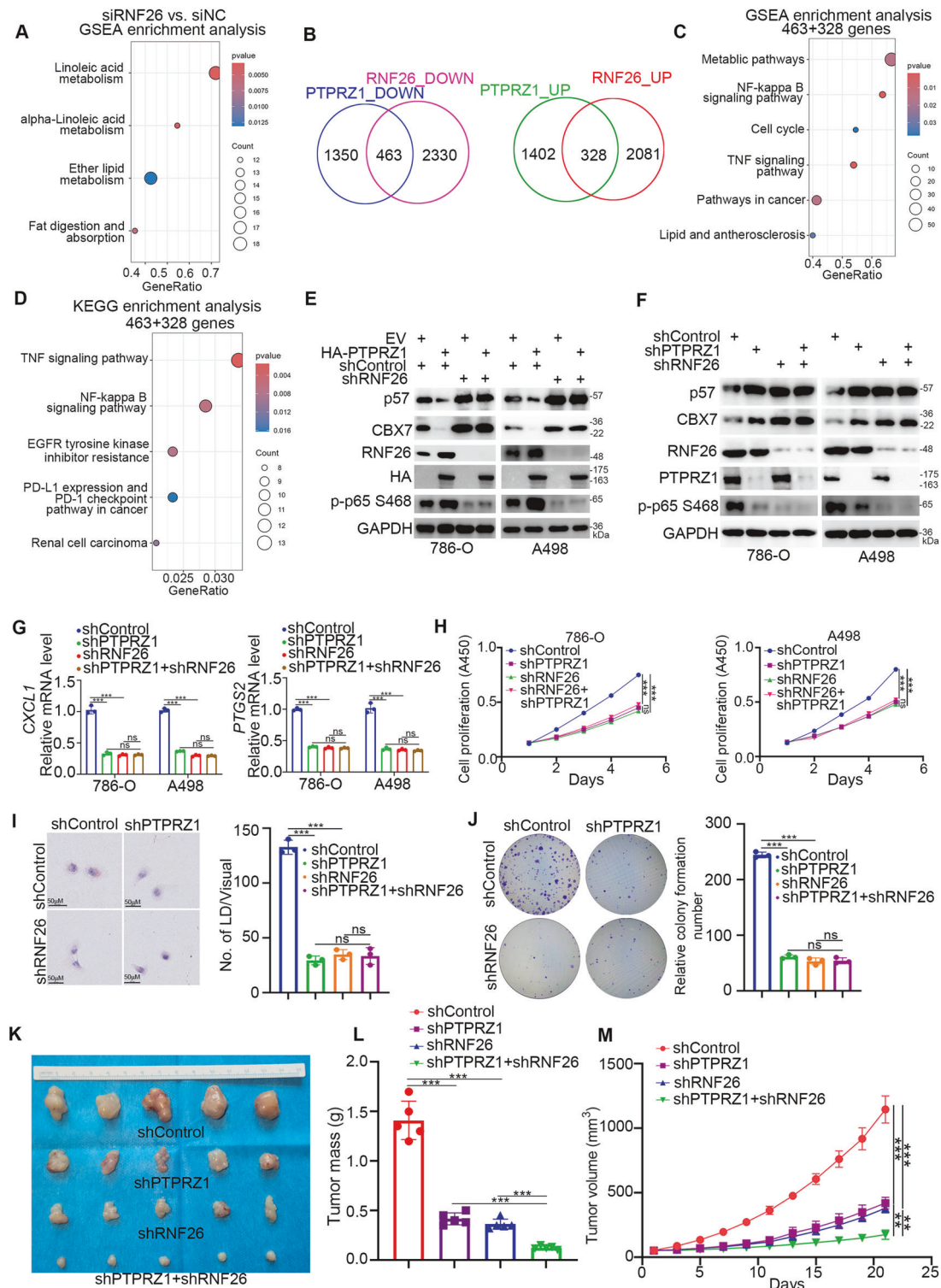
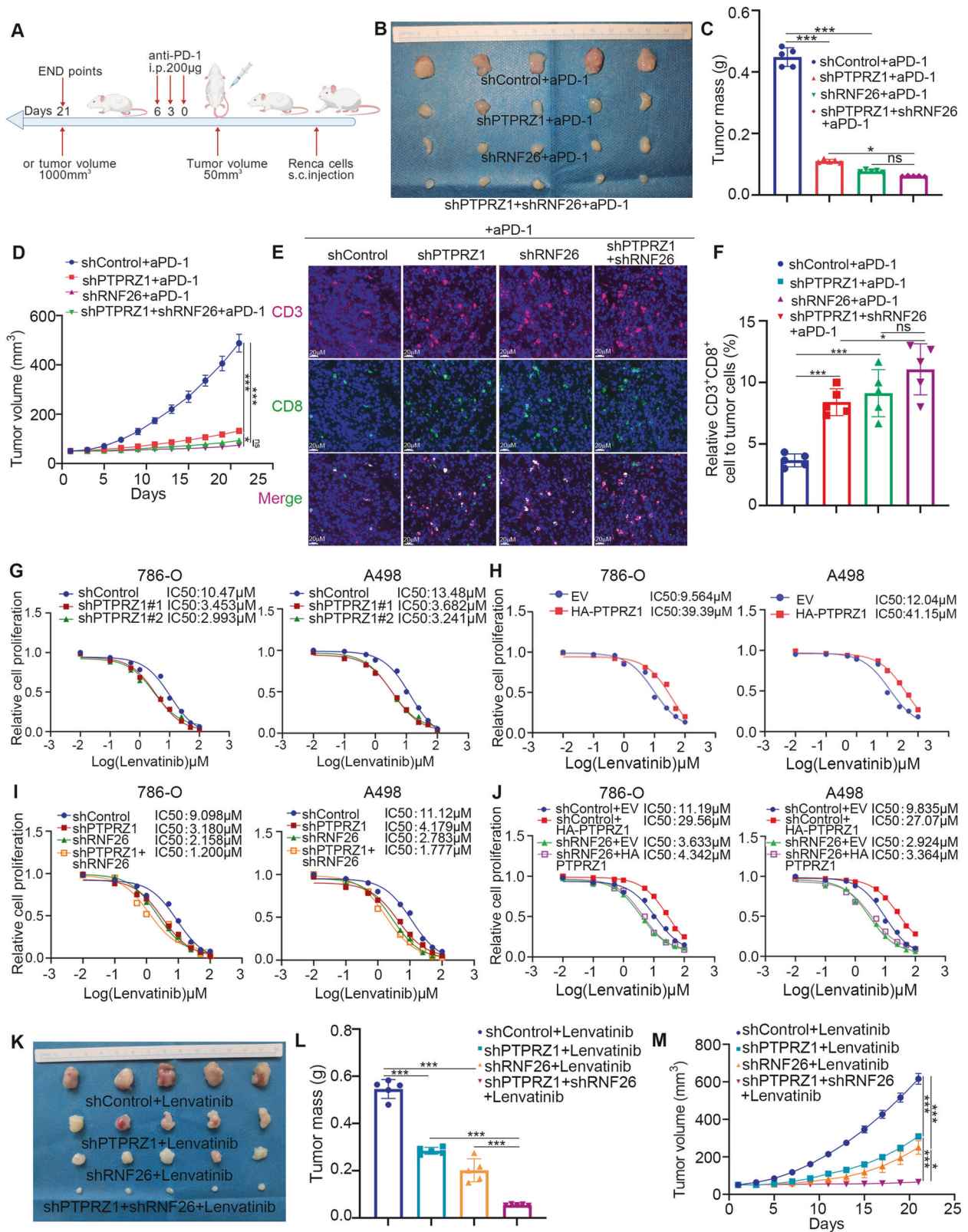


**Fig. 5 RNF26 is the key mediator for PTPRZ1 in ccRCC.** **A** GSEA enrichment analysis of RNA-seq after knockdown of RNF26 in A498 cells. **B–D** The venn diagram (**B**), GSEA enrichment analysis (**C**) and KEGG enrichment analysis (**D**) of common differential genes of RNA-seq after knockdown RNF26 and PTPRZ1. **E, F** 786-O and A498 cells were transfected with indicated plasmids for 24 h or shRNAs for 48 h, cells were harvested for western blot analysis. **G–J** 786-O and A498 cells were infected with indicated shControl, shPTPRZ1, shRNF26, or shPTPRZ1+shRNF26 for 72 h. The cells were harvested for the RT-qPCR analysis (**G**), CCK-8 assay (**H**), oil red staining (**I**), and colony formation assay (**J**). The scale bar indicated in the (**I**) is 50 µm. Data present as mean ± SD with three replicates. ns, not significant; \*\*\* $P < 0.0001$ . **K–M** A498 cells were infected with shControl, shPTPRZ1, shRNF26, or shPTPRZ1+shRNF26 for 72 h, the Puromycin was used to select shRNA-infected positive cells for 48 h. Then, cells were subcutaneously injected into the flank of nude mice. The xenografts were measured for 21 days. The tumour image is showed in (**K**), the tumour mass is showed in panel L, and tumour growth curve is showed in (**M**). Data presented as mean ± SD with six replicates. \*\* $P < 0.001$ ; \*\*\* $P < 0.001$ .



**Mouse experiments**

The Institutional Animal Care and Use Committee (IACUC) of the Second Xiangya Hospital, Central South University, thoroughly reviewed and approved all animal experiments conducted under the supervision of animal license number 20230475. These experiments adhered rigorously to the National Institutes of Health's Guide for the Care and Use of Laboratory Animals (NIH

Publications No. 8023, revised 1978). C57BL/6N mice (6 weeks old) were purchased from SJA Laboratory Animal Company (Changsha, China). BALB/C-nu/nu mice (6 weeks old) were purchased from SJA Laboratory Animal Company (Changsha, China). The mice were kept in standardized conditions, with a regulated 12 h light/dark cycle, and had unrestricted access to food and water. For cell manipulation, specific shRNA and shControl were used to infect

**Fig. 6 PTPRZ1 decreases the anti-tumor effect of ccRCC to TKIs and PD-1 blockade. A–F** A498 cells were transfected with indicated shRNAs for 72 h, the Puromycin was used to select shRNA-infected positive cells for 48 h, cells were subcutaneously injected into the flank of C57BL/6 mice. All of the mice were received anti-PD-1 treatments three times (tumor size reached 50 mm<sup>3</sup>, 3 days later, and 6 days later). The tumour image is showed in **(B)** the tumour mass is indicated in **(C)** and tumour growth curve is showed in **(D)**. Immunofluorescence staining was performed on the tumor tissues, and the image of CD3 + CD8 + T cells infiltration are showed in the figure E and F. Data were expressed as mean ± SD, three or five replicates. \*\*\**P* < 0.001. **G** A498 and 786-O cells were infected with shControl, shPTPRZ1#1, and shPTPRZ1#2 for 72 h. The puromycin was used to select shRNA-infected-positive cells for 48 h. Then, cells were subjected to measure the IC50 values of TKIs by treated with a serial dose of Lenvatinib for 24 h, and collected for colony formation assay. **H** 786-O and A498 cells were treated with inhibitor of PTPRZ1 and a serial dose of TKIs for 24 h. The IC50 values of Lenvatinib were showed in **(H. I)** 786-O and A498 cells were infected with shControl, shPTPRZ1, shRNF26, and shPTPRZ1+shRNF26 for 72 h, and the puromycin was used to select shRNA-infected-positive cells for 48 h. Then, cells were subjected to measure the IC50 values of TKIs by treated with a serial dose of Lenvatinib for 24 h. **J** 786-O and A498 cells were infected indicated shRNAs or plasmids. The puromycin was used to select shRNA-infected-positive cells for 48 h. Then, cells were subjected to measure the IC50 values of TKIs by treated with a serial dose of Lenvatinib for 24 h. **K–M** A498 cells were infected with indicated shRNAs for 72 h, and the puromycin was used to select shRNA-infected-positive cells for 48 h. Then, cells were subcutaneously injected into the flank of nude mice. All of the mice were received Lenvatinib treatments (20 mg/kg) after the tumour volume reached to 50 mm<sup>3</sup>. The tumour image is showed in **(K)** the tumour mass is indicated in **(L)**, and tumour growth curve is showed in **(M)**.

the cells over a period of 72 h. Following this, puromycin was administered for 48 h to select for cells positively expressing the shRNA. The transfected cells were then digested with trypsin and centrifuged at 1050 RPM for 5 min. After the addition of an adequate volume of PBS and thorough mixing, the cell suspension was kept on ice and promptly injected subcutaneously on the left dorsal side of the mice, at a density of  $5 \times 10^6$  cells per animal ( $n = 5$  mice per group). The tumor's growth was monitored by measuring its length and width every two days using a vernier caliper. The tumor volume was calculated using the formula  $(L \times W^2) / 2$ . Once the experimental timeline was completed, the mice were euthanized, and the tumors were excised, photographed, and weighed for further analysis.

### Immunohistochemistry (IHC)

Immunohistochemical analysis was conducted on the tissue microarray slides (#U081ki01, Bioaitech, Xian, China) utilizing primary antibodies specific to RNF26 (#16802-1-AP, Proteintech, Wuhan, China, 1:1000 dilution), and PTPRZ1 (#55125-1-AP, Proteintech, Wuhan, China, 1:2000 dilution). To assess the extent of antigen-antibody binding, a scoring system was implemented, which entailed multiplying the staining intensity by the percentage of positively stained cells. The staining intensity was categorized as follows: 0 representing no staining, 1 for light yellow (weak staining), 2 for yellow-brown (moderate staining), and 3 for brown (strong staining). This comprehensive scoring methodology provided a quantitative evaluation of the immunoreactivity within the tissue samples.

### Cell proliferation assay

To accurately assess cell proliferation, we employed the Cell Counting Kit-8 (CCK-8) assay. Cells were carefully seeded into 96-well plates and systematically categorized into distinct groups, each with varying treatments. To ensure statistical robustness, each group was replicated at least three times. Following this, 10 µl of CCK-8 reagent (#C0037, Beyotime, China) was precisely dispensed into each well, and the plates were incubated for a period of 2 h. Finally, the optical density (OD) at 450 nm was precisely measured using a microplate reader, providing a quantitative assessment of cell proliferation across the various treatment groups.

### Statistical analysis

The experimental data are presented in a concise and accurate manner, as the mean value accompanied by the standard error of the mean (mean ± SEM). The specific sample size ( $n$ ) for each statistical analysis is clearly indicated in the corresponding figure legends, ensuring transparency and reproducibility. To determine statistical significance, we employed appropriate statistical tests such as the Student's *t*-test, one-way ANOVA, or two-way ANOVA (in cases where more than two experimental groups were compared). A threshold of *P*-values less than 0.05 was set to indicate statistical significance. For ease of interpretation, we have adopted a widely recognized notation system to indicate the level of significance: ns, not significant; \**p* < 0.05; \*\**p* < 0.01; and \*\*\**p* < 0.001. This notation system provides a clear and intuitive representation of the statistical outcomes.

### DATA AVAILABILITY

The datasets used and/or analyzed during the current study are available from the corresponding authors on reasonable request.

### REFERENCES

- Moch H, Cubilla AL, Humphrey PA, Reuter VE, Ulbright TM. The 2016 WHO Classification of Tumours of the Urinary System and Male Genital Organs-Part A: Renal, Penile, and Testicular Tumours. *Eur Urol.* 2016;70:93–105.
- Ljungberg B, Albiges L, Abu-Ghanem Y, Bensalah K, Dabestani S, Fernandez-Pello S, et al. European Association of Urology Guidelines on Renal Cell Carcinoma: The 2019 Update. *Eur Urol.* 2019;75:799–810.
- Karam JA, Devine CE, Urbauer DL, Lozano M, Maity T, Ahrar K, et al. Phase 2 trial of neoadjuvant axitinib in patients with locally advanced nonmetastatic clear cell renal cell carcinoma. *Eur Urol.* 2014;66:874–80.
- Gossage L, Eisen T. Alterations in VHL as potential biomarkers in renal-cell carcinoma. *Nat Rev Clin Oncol.* 2010;7:277–88.
- Catalano M, De Giorgi U, Bimbatti D, Buti S, Procopio G, Sepe P, et al. Impact of Metastatic Site in Favorable-Risk Renal Cell Carcinoma Receiving Sunitinib or Pazopanib. *Clin Genitourin Cancer.* 2024;22:514–22.e511.
- Kase AM, George DJ, Ramalingam S. Clear Cell Renal Cell Carcinoma: From Biology to Treatment. *Cancers (Basel).* 2023;15:665.
- Vano YA, Elaidi R, Bennamoun M, Chevreau C, Borchiellini D, Pannier D, et al. Nivolumab, nivolumab-ipilimumab, and VEGFR-tyrosine kinase inhibitors as first-line treatment for metastatic clear-cell renal cell carcinoma (BIONIKK): a biomarker-driven, open-label, non-comparative, randomised, phase 2 trial. *Lancet Oncol.* 2022;23:612–24.
- Cremer T, Jongsma MLM, Trulsson F, Vertegaal ACO, Neeffes J, Berlin I. The ER-embedded UBE2J1/RNF26 ubiquitylation complex exerts spatiotemporal control over the endolysosomal pathway. *Cell Rep.* 2021;34:108659.
- Cremer T, Voortman LM, Bos E, Jongsma ML, Ter Haar LR, Akkermans JJ, et al. RNF26 binds perinuclear vimentin filaments to integrate ER and endolysosomal responses to proteotoxic stress. *EMBO J.* 2023;42:e111252.
- Lu X, Zhang Y, Wu Y, Lu T, Yang H, Yang W, et al. RNF26 Promotes Pancreatic Cancer Proliferation by Enhancing RBM38 Degradation. *Pancreas.* 2022;51:1427–33.
- Yi L, Wang H, Li W, Ye K, Xiong W, Yu H, et al. The FOXM1/RNF26/p57 axis regulates the cell cycle to promote the aggressiveness of bladder cancer. *Cell Death Dis.* 2021;12:944.
- Liu W, Wang H, Jian C, Li W, Ye K, Ren J, et al. The RNF26/CBX7 axis modulates the TNF pathway to promote cell proliferation and regulate sensitivity to TKIs in ccRCC. *Int J Biol Sci.* 2022;18:2132–45.
- He ZC, Liu Q, Yang KD, Chen C, Zhang XN, Wang WY, et al. HOXA5 is amplified in glioblastoma stem cells and promotes tumor progression by transcriptionally activating PTPRZ1. *Cancer Lett.* 2022;533:215605.
- Lorente G, Nelson A, Mueller S, Kuo J, Urfer R, Nikolich K, et al. Functional comparison of long and short splice forms of RPTPbeta: implications for glioblastoma treatment. *Neuro Oncol.* 2005;7:154–63.
- Nagai K, Fujii M, Kitazume S. Protein Tyrosine Phosphatase Receptor Type Z in Central Nervous System Disease. *Int J Mol Sci.* 2022;23:4414.
- Shang D, Xu X, Wang D, Li Y, Liu Y. Protein tyrosine phosphatase zeta enhances proliferation by increasing beta-catenin nuclear expression in VHL-inactive human renal cell carcinoma cells. *World J Urol.* 2013;31:1547–54.
- Wang V, Davis DA, Haque M, Huang LE, Yarchoan R. Differential gene up-regulation by hypoxia-inducible factor-1alpha and hypoxia-inducible factor-2alpha in HEK293T cells. *Cancer Res.* 2005;65:3299–306.

19. Liu YT, Shang D, Akatsuka S, Ohara H, Dutta KK, Mizushima K, et al. Chronic oxidative stress causes amplification and overexpression of ptpz1 protein tyrosine phosphatase to activate beta-catenin pathway. *Am J Pathol.* 2007;171:1978–88.
20. Fenech EJ, Lari F, Charles PD, Fischer R, Laetitia-Thezenas M, Bagola K, et al. Interaction mapping of endoplasmic reticulum ubiquitin ligases identifies modulators of innate immune signalling. *Elife.* 2020;9:e57306.
21. Ko PJ, Dixon SJ. Protein palmitoylation and cancer. *EMBO Rep.* 2018;19:e46666.
22. Peng Z, Cheng S, Kou Y, Wang Z, Jin R, Hu H, et al. The Gut Microbiome Is Associated with Clinical Response to Anti-PD-1/PD-L1 Immunotherapy in Gastrointestinal Cancer. *Cancer Immunol Res.* 2020;8:1251–61.
23. Li Y, Zhang L, Ren P, Yang Y, Li S, Qin X, et al. Qing-Xue-Xiao-Zhi formula attenuates atherosclerosis by inhibiting macrophage lipid accumulation and inflammatory response via TLR4/MyD88/NF- $\kappa$ B pathway regulation. *Phytomedicine.* 2021;93:153812.
24. Xu P, Sun Z, Wang Y, Miao C. Long-term use of indomethacin leads to poor prognoses through promoting the expression of PD-1 and PD-L2 via TRIF/NF- $\kappa$ B pathway and JAK/STAT3 pathway to inhibit TNF- $\alpha$  and IFN- $\gamma$  in hepatocellular carcinoma. *Exp Cell Res.* 2015;337:53–60.
25. Goldmann T, Otto F, Vollmer E. A receptor-type protein tyrosine phosphatase PTP zeta is expressed in human cutaneous melanomas. *Folia Histochem Cytobiol.* 2000;38:19–20.
26. Fu F, Xiao XI, Zhang T, Zou Q, Chen Z, Pei L, et al. Expression of receptor protein tyrosine phosphatase zeta is a risk factor for triple negative breast cancer relapse. *Biomed Rep.* 2016;4:167–72.
27. Ma Y, Ye F, Xie X, Zhou C, Lu W. Significance of PTPRZ1 and CIN85 expression in cervical carcinoma. *Arch Gynecol Obstet.* 2011;284:699–704.
28. Sethi G, Kwon Y, Burkhalter RJ, Pathak HB, Madan R, McHugh S, et al. PTN signaling: Components and mechanistic insights in human ovarian cancer. *Mol Carcinog.* 2015;54:1772–85.
29. Yamakawa T, Kurosawa N, Kadomatsu K, Matsui T, Itoh K, Maeda N, et al. Levels of expression of pleiotrophin and protein tyrosine phosphatase zeta are decreased in human colorectal cancers. *Cancer Lett.* 1999;135:91–6.
30. Laczminska I, Karpinski P, Bebenek M, Sedziak T, Ramsey D, Szmidka E, et al. Protein tyrosine phosphatase receptor-like genes are frequently hypermethylated in sporadic colorectal cancer. *J Hum Genet.* 2013;58:11–5.
31. Xia Z, Ouyang D, Li Q, Li M, Zou Q, Li L, et al. The Expression, Functions, Interactions and Prognostic Values of PTPRZ1: A Review and Bioinformatic Analysis. *J Cancer.* 2019;10:1663–74.
32. Ma L, Shen T, Peng H, Wu J, Wang W, Gao X. Overexpression of PTPRZ1 Regulates p120/beta-Catenin Phosphorylation to Promote Carcinogenesis of Oral Submucous Fibrosis. *J Oncol.* 2022;2022:2352360.
33. Kastana P, Ntenekou D, Mourkogianni E, Enake MK, Xanthopoulos A, Choleva E, et al. Genetic deletion or tyrosine phosphatase inhibition of PTPRZ1 activates c-Met to up-regulate angiogenesis and lung adenocarcinoma growth. *Int J Cancer.* 2023;153:1051–66.

## ACKNOWLEDGEMENTS

We would like to thank ProMab Biotechnologies, Inc. (Changsha, China) for their support with western blotting. Our schematic diagrams were created with BioRender.com.

## AUTHOR CONTRIBUTIONS

Yongkang Ma: Methodology; Wei Li: Methodology; Xinlin Liu: Methodology; Weilin Peng: Formal analysis; Bei Qing: Formal analysis; Shangqing Ren: Project administration; Wentao Liu: Methodology, Investigation; Xiaobing Chen: Project administration, Investigation.

## FUNDING

This work was supported by grants from the National Natural Science Foundation of China (Grant No. 82203537 (Wentao Liu)).

## COMPETING INTERESTS

The authors declare no competing interests.

## ETHICS APPROVAL AND CONSENT TO PARTICIPATE

The study was conducted in accordance with the principles of the Declaration of Helsinki principles. It was approved by the Animal Use and Care Committees at the Second Xiangya hospital, Central South University.

## CONSENT TO PUBLICATION

All subjects have written informed consent.

## ADDITIONAL INFORMATION

**Supplementary information** The online version contains supplementary material available at <https://doi.org/10.1038/s41388-024-03198-8>.

**Correspondence** and requests for materials should be addressed to Shangqing Ren, Wentao Liu or Xiaobing Chen.

**Reprints and permission information** is available at <http://www.nature.com/reprints>

**Publisher's note** Springer Nature remains neutral with regard to jurisdictional claims in published maps and institutional affiliations.

Springer Nature or its licensor (e.g. a society or other partner) holds exclusive rights to this article under a publishing agreement with the author(s) or other rightsholder(s); author self-archiving of the accepted manuscript version of this article is solely governed by the terms of such publishing agreement and applicable law.